# Fragmentation of $^{12}C$ projectiles interacting with $^{12}C$, $^{27}Al$, and $^{58}Ni$ nuclei at energy 28.7 MeV/nucleon

J. Czudek, L. Jarczyk, B. Kamys, A. Magiera, R. Siudak, A. Strzałkowski, and B. Styczeń
*Institute of Physics, Jagellonian University, Cracow, Poland*

J. Hebenstreit,* W. Oelert, P. von Rossen, and H. Seyfarth
*Institut für Kernphysik, Forschungszentrum Jülich, Federal Republic of Germany*

A. Budzanowski and A. Szczurek
*Institute of Nuclear Physics, Cracow, Poland*
(Received 29 June 1990)

Inclusive spectra of different isotopes of He, Li, Be, B, C, and N nuclei emerging from the collisions of $^{12}C$ ions of energy 344.5 MeV with carbon, aluminum, and nickel target nuclei have been measured in the angular range of 4°–36° (laboratory). Experimental yields of reaction products are almost the same for the different targets. The continuous parts of momentum spectra have been decomposed into three components, corresponding to direct and damped fragmentation and to other processes, such as deep-inelastic and/or compound-nucleus reactions. At small angles (smaller than 20° in the laboratory system) the fragmentation processes dominate whereas at larger angles they become negligible in comparison to the other components. The direct fragmentation contribution is very small with respect to the damped one. The obtained reduced momentum widths of the direct fragmentation bumps are significantly smaller than those predicted by the Goldhaber model but agree with results obtained from other experiments at similar energies.

## I. INTRODUCTION

Heavy-ion reactions at low energies ($<10$ MeV/nucleon) were studied intensively for the past two decades. A large body of the analyzed experimental data shows that these reactions are dominated by quasielastic and deep-inelastic processes as well as compound nucleus formation. At higher energies it was found that fragmentation plays an important role.[1–5]

At the intermediate-energy region, the mean-field description is on the decline and the nucleonic degrees of freedom start to be important. Thus, various reaction mechanisms may be expected here, from quasielastic processes[6–8] and mass-transfer processes,[9] through complete and incomplete fusion[10–13] to fragmentation.[14–18]

It is the aim of this work to study the mechanism of the reactions induced by $^{12}C$ projectiles on different targets at the incident energy close to the Fermi energy. The inclusive spectra of various ejectiles emerging from the collisions of $^{12}C$ ions with carbon, aluminum, and nickel target nuclei have been measured in a broad angular range (4°–36° laboratory) at the incident energy 28.7 MeV/nucleon. The experimental procedure and results are discussed in Sec. II of this paper.

In order to find the contribution from fragmentation processes, we used a simple model proposed recently by Seres *et al.*[19] In Sec. III, a decomposition of the momentum spectra into contributions from projectile fragmentation (direct and damped) and other processes (e.g., deep-inelastic or fully damped) has been performed for all the spectra according to Ref. 19. An analysis of angular dependences of parameters of the model, obtained for all ejectiles under consideration, is presented and gross properties of different components of the momentum spectra are discussed in detail. The conclusions are given in Sec. IV.

## II. EXPERIMENTAL PROCEDURE AND RESULTS

The $^{12}C$ ions produced in the ISIS ion source[20] were accelerated to the energy 344.5 MeV in the JULIC cyclotron of the Forschungszentrum Jülich. The beam was focused onto self-supporting targets of $^{12}C$, $^{27}Al$, and $^{58}Ni$ with thicknesses of 1.1, 1.3, and 0.5 mg/cm$^2$, respectively. The reaction products were detected in telescopes consisting of 50-$\mu$m-, 400-$\mu$m-, 2-mm-, and 6-mm-thick Si surface-barrier detectors. The solid angle covered by the detectors was 0.04 msr. The detectors were cooled to the temperature $-20$ °C. The telescopes allowed us to obtain very good $(A,Z)$ resolution in the whole measured energy range and to achieve low-energy thresholds for the detected particles (20–30 MeV for alpha particles and 50–60 MeV for $^{12}C$ ejectiles). The energy resolution was 600–700 keV. The absolute calibration of the energy scale was performed in two steps. In the first one the relative adjustment of the electronic tracts of all detectors was done using the pulses from the 400-$\mu$m detector corresponding to the elastic-scattering line from the gold target. Finally, the calibration was estimated from known

 

energies of discrete peaks from different reactions. The obtained accuracy was around 2 MeV.

For identification of different ejectiles, the identification parameter was formed according to Ref. 21,

$$p=(\Delta E+E)^b-E^b$$

from the pulses $\Delta E$ and $E$ from the transmission and stopping detectors, respectively. In this formula, $b=B-C\Delta E/D$, $B=1.7943$, $C=4.2162\times10^{-2}$ $\mu$m/MeV, and $D$ denotes the thickness of the transmission counter in $\mu$m. A typical identification spectrum is presented in Fig. 1.

The energy spectra of all stable ejectiles starting from $^3$He up to $^{15}$N have been measured at laboratory angles from 4° to 11.5° in 0.5° steps for the $^{12}$C, $^{27}$Al, and $^{58}$Ni targets while the angular range was extended to 36° in 1° steps for the $^{12}$C and $^{27}$Al targets. The absolute cross sections were evaluated from the measured counting rates, target thicknesses, solid angle of the detecting system, and integrated beam charge. The uncertainty in absolute normalization of cross section was estimated to be ±7%.

Typical examples of ejectile momentum spectra are shown in Figs. 2–4. In Fig. 2, spectra of $^9$Be fragments produced in the $^{12}$C+$^{27}$Al interaction are presented for the three different angles: 5.5°, 15°, and 36° (laboratory). The target dependence of momentum spectra is illustrated in Fig. 3 where the $^9$Be-fragment spectra measured at 5.5° are shown for all the targets. Spectra of various fragments measured at 5.5° for the $^{27}$Al target are depicted in Fig. 4. All the spectra at forward angles show a pronounced asymmetric bump at the momentum corresponding approximately to the beam velocity. This bump disappears at large angles where the spectra exhibit an exponential dependence on the ejectile momentum (Fig. 2). The momentum spectra of boron, carbon, and nitro-

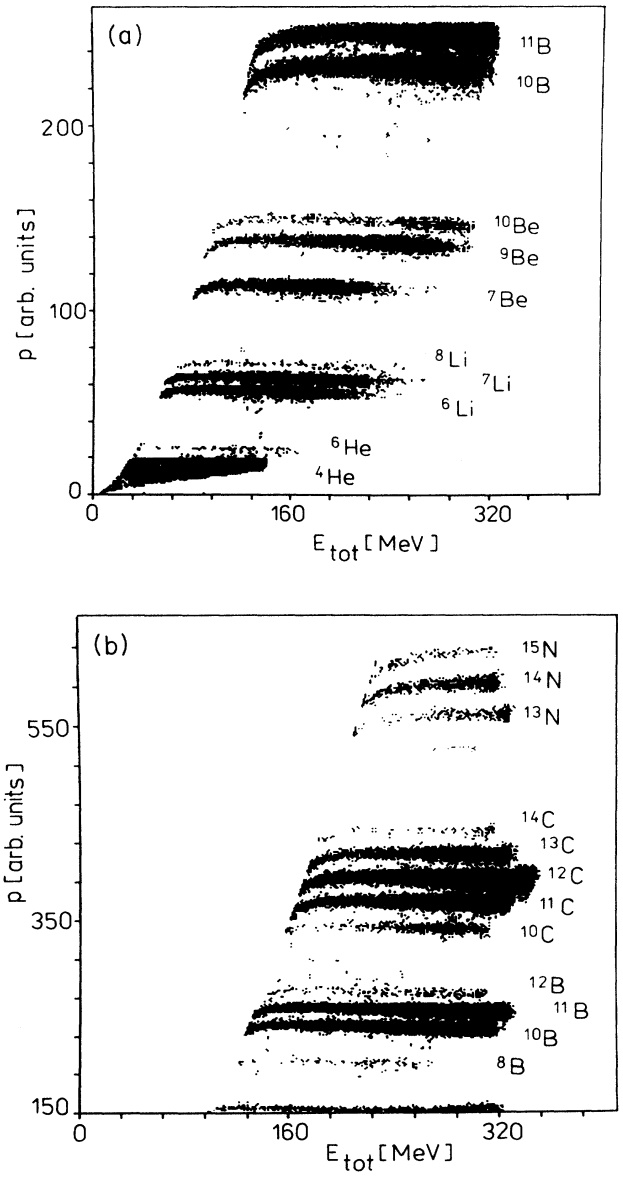


FIG. 1. The sample of the identification spectrum for lower and higher mass fragments.

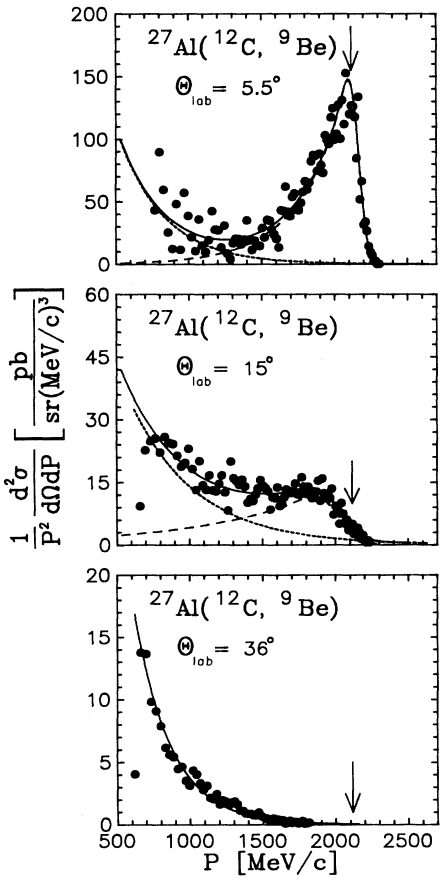


FIG. 2. Spectra of $^9$Be measured for the $^{12}$C+$^{27}$Al reaction at various angles. The dashed line represents the fragmentation contribution, the dotted curve the background from other processes, and the solid curve the sum of both contributions. The arrows indicate the momenta corresponding to the beam velocity.

gen ejectiles also contain a few narrow, discrete peaks due to quasielastic reactions as illustrated in Fig. 5. Except for these peaks, the spectra have very similar behavior for all targets investigated.

In Fig. 6 the total cross sections obtained by the integration of measured momentum spectra over the investigated energy and angular range are shown for all ejectiles for the $^{12}C$ and $^{27}Al$ targets. Peaks corresponding to transitions to discrete states were excluded from the energy integration. The very similar yields of various ejectiles for both targets indicate that the mechanism of the reaction is almost independent of the target. This may be interpreted as an indication that the mechanism of the reaction is dominated by projectile fragmentation. Furthermore, one can find a strong correlation of the yields of reaction products with the $Q$ value of the binary decay of the $^{12}C$ projectile (assuming fragments in their ground states), as shown in Fig. 7 for $^{12}C$ (circles) and $^{27}Al$ (squares) targets. The yields decrease nearly exponentially as the $Q$ value increases. Similar behavior has been recently observed by the Berkeley group.[22]

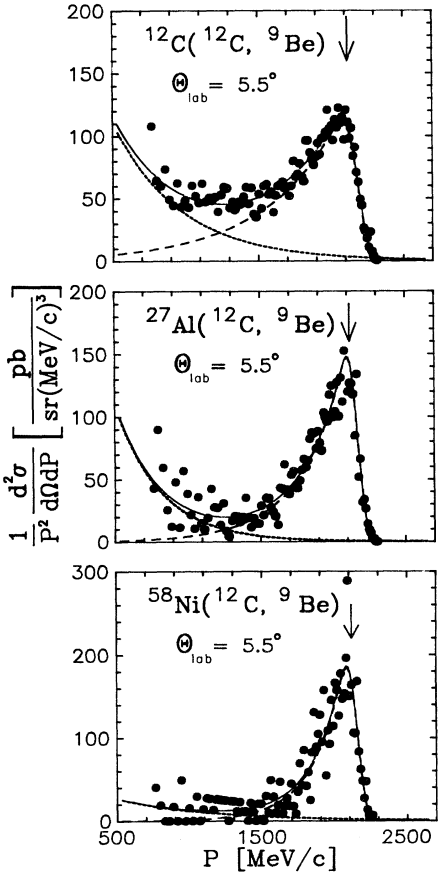


FIG. 3. Spectra of $^{9}Be$ fragments at 5.5° for different targets. The dashed line represents the fragmentation contribution, the dotted curve the background component, and the solid curve the sum of both contributions. The arrows indicate the momenta corresponding to the beam velocity.

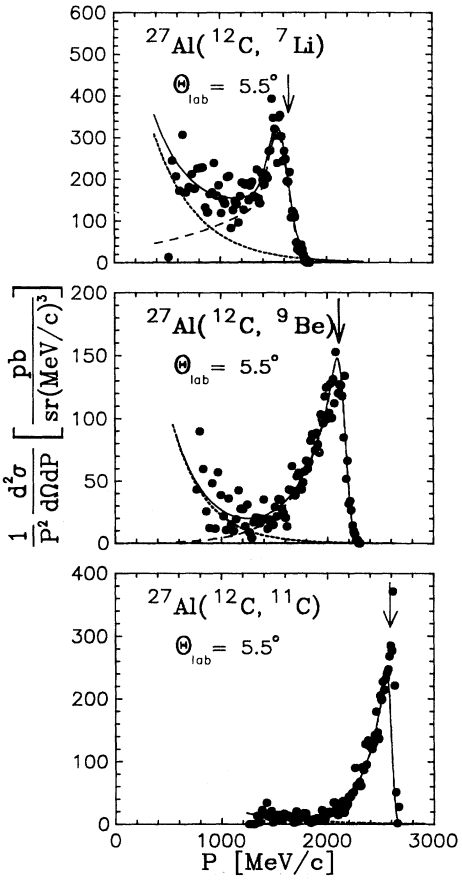


FIG. 4. Spectra of different fragments at 5.5° for the $^{27}Al$ target. The dashed line represents the fragmentation contribution, the dotted line the background component, and the solid line the sum of both contributions. The arrows indicate the momenta corresponding to the beam velocity.

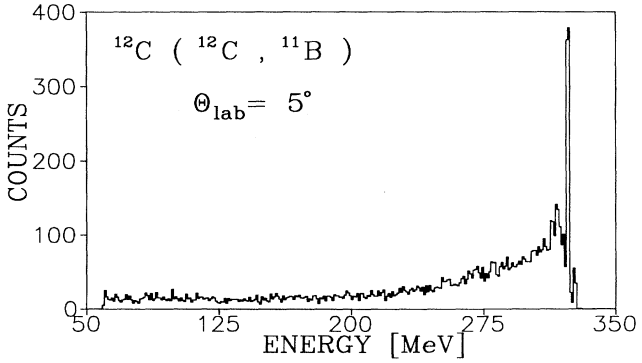


FIG. 5. Spectrum of $^{11}B$ ejectile from $^{12}C+^{12}C$ interaction emitted at angle 5°. Apart from a continuous fragmentation part the peaks corresponding to quasielastic processes are visible.

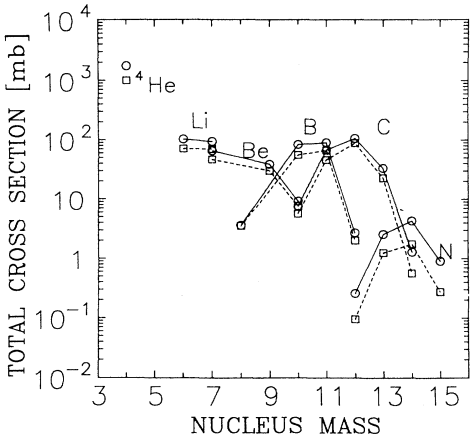


FIG. 6. Energy- and angle-integrated yields for all measured isotopes for $^{12}$C (circles) and $^{27}$Al (squares) targets. Peaks corresponding to transitions to discrete states were excluded. The solid ($^{12}$C) and dashed ($^{27}$Al) lines are drawn to guide the eye.

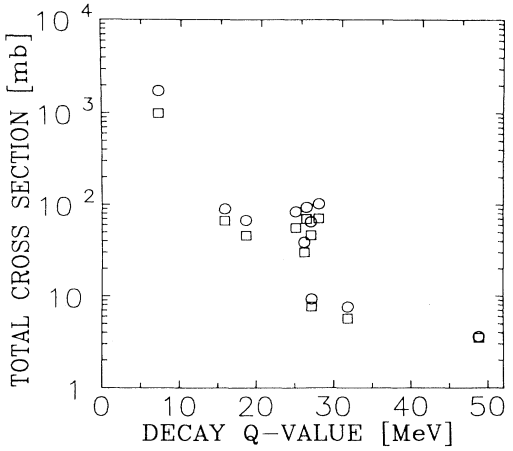


FIG. 7. The cross section obtained by the integration over the measured energy and angular ranges for all measured ejectiles for the $^{12}$C (circles) and $^{27}$Al (squares) target as a function of the projectile binary decay $Q$ value.

## III. ANALYSIS OF THE MOMENTUM SPECTRA

The shape of the experimental momentum spectra, i.e., the presence of the asymmetric bump at the momentum corresponding to the beam velocity, and its approximate independence of the target suggests the mechanism of projectile fragmentation accompanied by dissipation processes.

The simple parametrization of the momentum spectra taking into account fragmentation of the projectile and the energy dissipation processes, has been recently proposed by Seres *et al.*[19] The parametrization has been derived under the following assumptions.

(i) Fragmentation leads to a Gaussian momentum distribution of fragments with centroid at momentum $p_0$ and with standard deviation $\sigma$.

(ii) The "direct" fragmentation occurs in a fraction "$w$" of all fragmentation events while, in the remaining $(1-w)$ fraction, the fragments interact, thereby decreasing their momentum. The probability distribution of the loss of momentum in the damping process is described by an exponential function with parameter $q$.

(iii) Momentum spectra of projectiles emitted in more complicated processes (later called background), e.g., deep-inelastic scattering and fully damped collisions, are parametrized by an exponential function with parameters $h$ and $\beta$.

The resulting formula is as follows:

$$p^{-2}\frac{d^2\sigma}{d\Omega\, dp}=\frac{wg_0}{\sqrt{2\pi}\sigma}\exp\left[-\frac{(p-p_0)^2}{2\sigma^2}\right]+\frac{(1-w)g_0}{q}\exp\left[\frac{\sigma^2}{2q^2}+\frac{p-p_0}{q}\right]\times\left[1-\mathrm{erf}\left[\frac{p-p_0+\sigma^2q^{-1}}{\sigma}\right]\right]+h\beta\exp(-\beta p)\,, \quad (1)$$

where erf($x$) denotes the error function. The first term in the sum corresponds to the direct fragmentation process (i), the second term describes the contribution from fragmentation with energy dissipation (ii), and the last term (iii) is a background connected with other processes.

It should be noted that, while formula (1) for the fragmentation spectrum has been derived under the assumption of momentum damping after fragmentation, a similar formula can be obtained assuming that the damping occurs before fragmentation. Numerical calculations show that both formulas give almost the identical cross section. Therefore, in an inclusive experiment, we cannot distinguish whether damping occurs before or after fragmentation. In order to make our results comparable to those of Seres *et al.*,[19] further analysis was made using formula (1).

Parametrization (1) has been used to describe the continuous part of inclusive momentum spectra of $^6$Li, $^7$Li, $^7$Be, $^9$Be, $^{10}$Be, $^8$B, $^{10}$B, $^{11}$B, $^{10}$C, and $^{11}$C particles produced in collisions of $^{12}$C projectiles with $^{12}$C, $^{27}$Al, and $^{58}$Ni nuclei at $E_{\mathrm{lab}}=344.5$ MeV. The parameters $g_0$, $p_0$, $\sigma$, $w$, $q$, $\beta$, and $h$ were obtained from fitting the model momentum distribution (1) to the experimental spectra for each ejectile at different angles in the range from 4° to 36° (laboratory). The narrow peaks corresponding to the quasielastic transitions to discrete states were not taken into account in the fitting procedure.

The parameters $p_0$ and $\sigma$ were determined uniquely by the right flank of the momentum spectrum. It was found that the $w$ parameter has, in all cases, a very small value and does not influence the estimation of the $g_0$ and $q$ parameters. The background parameters $\beta$ and $h$ in small-angle spectra do not affect the fragmentation part.

It has been found that, by employing parametrization (1), it is possible to reproduce the continuous part of the experimental spectra for all targets, fragments and angles. The quality of the fits is illustrated in Figs. 2–4. The contributions corresponding to the fragmentation

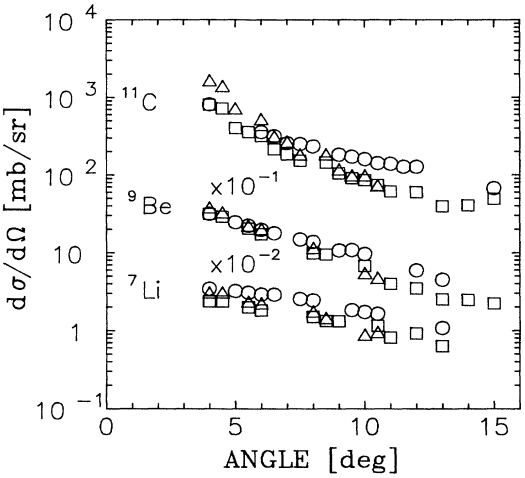


FIG. 8. Angular distributions of the fragmentation cross section for selected fragments. The circles denote angular distributions for the $^{12}$C target, the squares for the $^{27}$Al target, and the triangles for the $^{58}$Ni target.

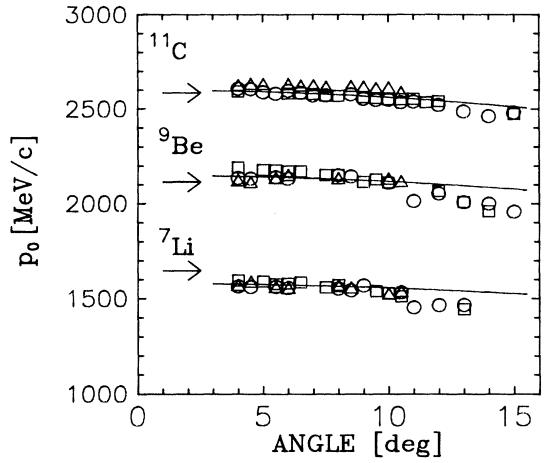


FIG. 10. Parameter $p_0$ as a function of laboratory angle for selected fragments and all the targets. The circles denote ejectile angular distributions for the $^{12}$C target, the squares for $^{27}$Al, and the triangles for the $^{58}$Ni target. The arrows correspond to the beam velocity. Additionally, the $\cos\vartheta$ dependence normalized to the experimental data at forward angles is plotted with the solid curves.

[(i)+(ii)] and those corresponding to other processes [(iii)] are shown separately. The dashed line represents the fragmentation, the dotted curve the background component, while the solid line corresponds to the sum of both contributions. The momenta corresponding to the beam velocity are marked by the arrows.

A good reproduction of the experimental momentum spectra when using parameters varying smoothly with the scattering angle confirms that the fragmentation of the projectile is the dominant mechanism of the reaction. Typical behavior of the angular dependence of the parameters is shown in Figs. 7–10.

The momentum-integrated cross section for fragmentation is mainly determined by the value of the $g_0$ parameter. The angular distributions of fragmentation, obtained by a numerical integration of the two fragmentation contributions [(i)+(ii)] in formula (1), are presented in Fig. 8 for representative fragments. The circles denote angular distributions for the $^{12}$C target, the squares for $^{27}$Al target, and the triangles for the $^{58}$Ni target. All angular distributions are smooth, approximately exponential functions of angle and very similar for the different targets.

The analysis performed indicates that the damped fragmentation dominates. The direct fragmentation probability $w$ is small ($<0.3$), being on the average larger for heavier targets. In the cases of $^{11}$B and $^{11}$C ejectiles, $w$ is practically zero, while for the other ejectiles, $w$ is a rapidly decreasing function of angle.

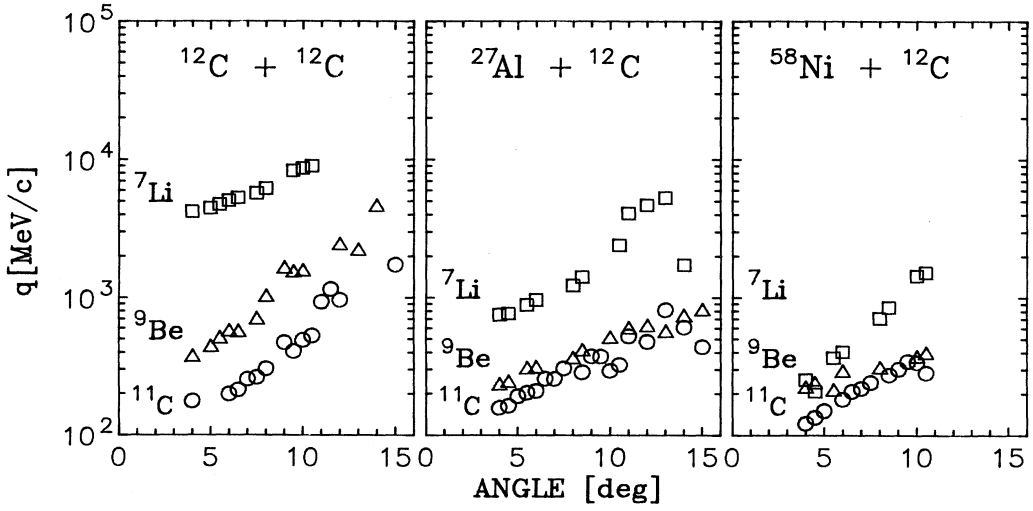


FIG. 9. The damping parameter $q$ as a function of angle for $^{12}$C, $^{27}$Al, and $^{58}$Ni targets. Squares are for $^7$Li, triangles for $^9$Be, and circles for $^{11}$C fragments.

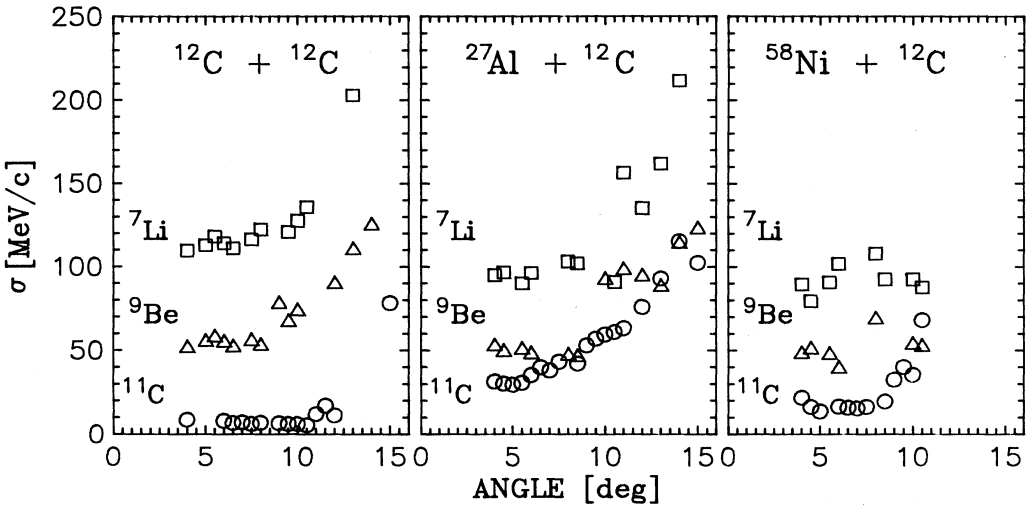


FIG. 11. Angular dependence of $\sigma$ for $^{12}C$, $^{27}Al$, and $^{58}Ni$ targets. Squares are for $^{7}Li$, triangles for $^{9}Be$, and circles for $^{11}C$ fragments.

The parameter $q$ describing the damping of the momentum in the fragmentation process is an increasing function of the angle (Fig. 9), which is typical for dissipation processes. However, it surprisingly depends strongly on both target and ejectile. It changes continuously from target to target, being the largest for light fragments produced in reactions with the $^{12}C$ target.

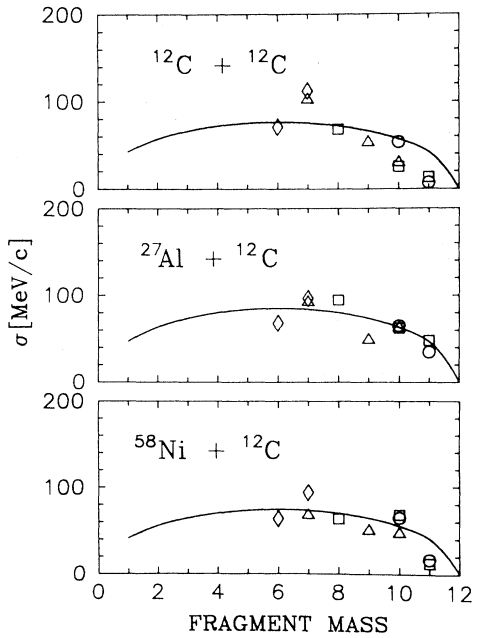


FIG. 12. The dependence of $\sigma$ on fragment mass for all targets ($\sigma$ averaged over the angular interval 4°–8°). The various symbols denote the following ejectiles: diamonds, Li; triangles, Be; squares, B; circles, C. The solid line corresponds to the prediction of the Goldhaber model (Ref. 17) with the reduced width $\sigma_0$=42.4, 47.0, and 41.1 MeV/$c$, fitted to the experimental data for $^{12}C$, $^{27}Al$, and $^{58}Ni$ targets, respectively.

The parameter $p_0$, the centroid of the direct fragmentation bump, practically does not depend on the target (see Fig. 10). For forward angles it is very close to the momentum corresponding to the beam velocity marked by arrows in Fig. 10. The slope of the angular dependence of $p_0$ is only slightly steeper than one may expect from a simple $\cos\vartheta$ dependence, shown by the solid curves, which may be obtained at higher energy.[1] A similar effect has been found in Ref. 23.

The parameter $\sigma$ which determines the width of the direct fragmentation bump is practically constant in the interval 4°–8° and rises at larger angles (see Fig. 11). This effect depends both on the fragment and on the target. The rise is stronger for lighter fragments. For a spherically symmetric, three-dimensional Gaussian momentum distribution of clusters in the projectile, neglecting interaction with the target and the residual part of projectile, $\sigma$ should be angle independent. The observed effect may be interpreted as asymmetry of momentum distribution of clusters in the projectile due to the interaction with the target and/or a residual part of the projectile.[17,24]

Figure 12 shows the dependence of $\sigma$, averaged over the angular interval 4°–8°, on the fragment mass for all targets. Fitting $\sigma$ to the experimental values according to the scaling law of Goldhaber,[4] we get the reduced width $\sigma_0$=42.4, 47.0, and 41.1 MeV/$c$ for $^{12}C$, $^{27}Al$, and $^{58}Ni$ targets, respectively. These values are significantly smaller than those found from the high-energy limit (about 100 MeV/$c$).[17] It cannot be explained by the influence of the Coulomb interaction according to the peripheral model of Friedman[5] or by the model proposed by Bonasera *et al.*[17] However, it should be pointed out that the obtained $\sigma_0$ values are consistent with experimental systematics (see, e.g., Refs. 25 and 26).

The simple parametrization of the background component does not prejudge the underlying reaction mechanism. A few mechanisms may contribute, like evaporation after complete and incomplete fusion, deep-inelastic

processes, and target fragmentation. These processes should be strongly target dependent. Indeed, we observe large differences of the background for different targets (see Fig. 3). For instance, in the case of the $^{12}C+^{12}C$ system, the background may be caused by a contribution from compound nucleus mechanism. It is very likely that, for such a light system, evaporation residue can contribute significantly to the low-momentum part of the spectra. This effect should not be observed for heavier systems in the measured energy range because energy corresponding to the velocity of the compound system is below the experimental energy threshold.

## IV. CONCLUSIONS

The following conclusions may be drawn from the present analysis of the experimental momentum spectra of different ejectiles produced in reactions induced by $^{12}C$ projectiles at energy 28.7 MeV/nucleon.

The high-energy parts of the spectra at forward angles are dominated by fragmentation processes. The following arguments support that conclusion: (a) the presence of the pronounced bump in all spectra at the momenta corresponding to beam velocity, (b) the very weak dependence of yields of various ejectiles on the target nucleus, (c) strong correlation of the measured fragment yields with the $Q$ values of binary decays of the $^{12}C$ projectile into the observed fragments, and (d) the fact that the experimental momentum spectra are well reproduced by the simple parametrization based on the assumption of projectile fragmentation. Values of the parameters of this phenomenological parametrization vary smoothly with the reaction angle.

The analysis leads to the conclusion that damped fragmentation dominates. This damping increases rapidly with the reaction angle.

The reduced widths $\sigma_0$ of the momentum distribution extracted from the analysis are significantly smaller than those obtained at higher energies ( $>100$ MeV/nucleon). However, they agree with results obtained by other authors at similar energies.

This work was supported in part by Polish Ministry of National Education under Contract CPBP 01.09.

*On leave from the Jagellonian University, Cracow, Poland.

[1]D. E. Greiner, P. J. Lindstrom, H. H. Heckmann, Bruce Cork, and F. S. Bieser, Phys. Rev. Lett. **35**, 152 (1975).
[2]J. Coguon and R. Sartov, Phys. Rev. C **21**, 2342 (1980).
[3]D. L. Olson, B. L. Berman, D. E. Greiner, H. H. Heckman, P. J. Lindstrom, and H. J. Crawford, Phys. Rev. C **28**, 1602 (1983).
[4]A. S. Goldhaber, Phys. Lett. **53B**, 306 (1974).
[5]W. A. Friedman, Phys. Rev. C **27**, 569 (1983).
[6]M. C. Mermaz, Phys. Lett. **155B**, 330 (1985).
[7]M. C. Mermaz, R. Dayras, J. Barrette, B. Bethier, D. M. de Castro Rizzo, O. Cisse, R. Legrain, A. Pagano, E. Pollacco, H. Delagrange, W. Mittig, B. Heusch, G. Lanzano, and A. Palmeri, Nucl. Phys. **A441**, 129 (1985).
[8]M. C. Mermaz, Phys. Rev. C **36**, 1000 (1987).
[9]Y. Miyama and T. Kammuri, Prog. Theor. Phys. **77**, 1209 (1987).
[10]A. J. Cole, Z. Phys. A **322**, 315 (1985).
[11]L. G. Moretto and G. J. Wozniak, *Progress in Particle and Nuclear Physics* (Pergamon, Oxford, 1988), Vol. 21, p. 401.
[12]J. Wilczyński, K. Siwek-Wilczyńska, J. van Driel, S. Gonggrijp, D. C. J. M. Hageman, R. V. F. Janssens, J. Łukasiak, and R. H. Siemssen, Phys. Rev. Lett. **45**, 606 (1980).
[13]H. Morgenstern, W. Bohne, W. Galster, K. Grabisch, and A. Kyanowski, Phys. Rev. Lett. **52**, 1104 (1984).
[14]C. Guet, Nucl. Phys. **A400**, 191C (1983).
[15]V. Borrel, D. Guerreau, J. Galin, B. Gatty, D. Jacquet, and X. Tarrago, Z. Phys. A **314**, 191 (1983).
[16]V. Borrel, B. Gatty, D. Guerreau, J. Galin, and D. Jacquet, Z. Phys. A **324**, 205 (1986).
[17]A. Bonasera, M. di Toro, and C. Grégoire, Nucl. Phys. **A463**, 653 (1987).
[18]K. Möhring, T. Srokowski, D. H. E. Gross, and H. Homeyer, Phys. Lett. B **203**, 210 (1988).
[19]Z. Seres, F. Deak, A. Kiss, G. Caskey, A. Galonsky, L. Heilbronn, and B. Remington, Nucl. Phys. **A492**, 315 (1989).
[20]H. Beuscher *et al.*, Jülich Annual Report IKP KFA Juel. Spez. **442**, 105, 1987.
[21]F. S. Goulding, in *Treatise on Heavy Ion Science*, edited by D. A. Bromley (Plenum, New York, 1985), Vol. 7, p. 235.
[22]R. G. Stokstad, Y. D. Chan, A. Dacal, D. E. Di Gregorio, B. A. Harmon, R. Knop, M. E. Ortiz, E. Plagnol, J. Pouliot, C. Moisan, L. Potvin, C. Rioux, and R. Roy, Lawrence Berkeley Laboratory Report 25810, 1988.
[23]A. Kiss, F. Deak, Z. Seres, G. Caskey, A. Galonsky, B. Remington, and L. Heilbronn, Nucl. Phys. **A499**, 131 (1989).
[24]R. Dayras, A. Pagano, J. Barrette, B. Berthier, D. M. de Castro Rizzo, E. Chavez, O. Cisse, R. Legrain, M. C. Mermaz, E. C. Pollacco, H. Delagrange, W. Mittig, B. Heusch, R. Coniglione, G. Lanzano, and A. Palmeri, Nucl. Phys. **A460**, 299 (1986).
[25]F. Rami, J. P. Coffin, G. Guillaume, B. Heusch, P. Wagner, A. Fahli, and P. Fintz, Nucl. Phys. **A444**, 325 (1985).
[26]Y. Blumenfeld, Ph. Chomaz, N. Frascaria, J. P. Garron, J. C. Jacmart, J. C. Roynette, D. Ardouin, and W. Mittig, Nucl. Phys. **A455**, 357 (1986).